Title

Emissive Synthetic Cofactors: A Highly Responsive NAD+ Analogue Reveals Biomolecular Recognition Features

Journal

Chemistry - A European Journal, 25(17)

ISSN

0947-6539

Authors

Feldmann, Jonas
Li, Yao
Tor, Yitzhak

Publication Date

2019-03-21

DOI

10.1002/chem.201805520

Peer reviewed

HHS Public Access

Author manuscript

Chemistry. Author manuscript; available in PMC 2020 January 06.

Published in final edited form as:

Chemistry. 2019 March 21; 25(17): 4379–4389. doi:10.1002/chem.201805520.

Emissive Synthetic Cofactors: A Highly Responsive NAD+ Analogue Reveals Biomolecular Recognition Features**

Jonas Feldmann[a],[b], **Yao Li**[a], **Yitzhak Tor**[a]

[a]Department of Chemistry and Biochemistry, University of California San Diego, La Jolla, CA 92093-0358 (USA)

[b]Department of Chemistry, Ludwig-Maximilians-Universität München Butenandtstr. 5–13, 81377 Munich (Germany)

Abstract

Apart from its vital function as a redox cofactor, nicotinamide adenine dinucleotide (**NAD**$^+$) has emerged as a crucial substrate for **NAD**$^+$-consuming enzymes, including poly(ADP-ribosyl)transferase 1 (PARP1) and CD38/CD157. Their association with severe diseases, such as cancer, Alzheimer's disease, and depressions, necessitates the development of new analytical tools based on traceable **NAD**$^+$ surrogates. Here, the synthesis, photophysics and biochemical utilization of an emissive, thieno[3,4-*d*]pyrimidine-based **NAD**$^+$ surrogate, termed **NthAD**$^+$, are described. Its preparation was accomplished by enzymatic conversion of synthetic **thATP** by nicotinamide mononucleotide adenylyltransferase 1 (NMNAT1). The new NAD$^+$ analogue possesses useful photophysical features including redshifted absorption and emission maxima as well as a relatively high quantum yield. Serving as a versatile substrate, **NthAD**$^+$ was reduced by alcohol dehydrogenase (ADH) to **NthADH** and afforded thADP-ribose (**thADPr**) upon hydrolysis by **NAD**$^+$-nucleosidase (NADase). Furthermore, **NthAD**$^+$ was engaged in cholera toxin A (CTA)-catalyzed mono(thADP-ribosyl)ation, but was found incapable in promoting PARP1-mediated poly(thADP-ribosyl)ation. Due to its high photophysical responsiveness, **NthAD**$^+$ is suited for spectroscopic real-time monitoring. Intriguingly, and as an N7-lacking NAD$^+$ surrogate, the thieno-based cofactor showed reduced compatibility (i.e., functional similarity compared to native **NAD**$^+$) relative to its isothiazolo-based analogue. The distinct tolerance, displayed by diverse NAD$^+$ producing and consuming enzymes, suggests unique biological recognition features and dependency on the purine N7 moiety, which is found to be of importance, if not essential, for PARP1-mediated reactions.

Keywords

ADP-ribosylation; cofactors; NAD$^+$; PARP1; spectroscopy

[**]*NAD*$^+$ = oxidized nicotinamide adenine dinucleotide.

ytor@ucsd.edu.

Conflict of interest

The authors declare no conflict of interest.

Introduction

The most prominent role of nicotinamide adenine dinucleotide (**NAD**$^+$, Figure 1) is as a redox cofactor in regulating central metabolic pathways by catalyzing a variety of oxidoreductase-mediated processes[1] Moreover, **NAD**$^+$ has been recently found to act as a substrate for multiple enzymes that catalyze glycosidic cleavage of the nicotinamide moiety and release an ADP-ribose (**ADPr**) moiety, which is then transferred onto acceptor molecules, such as proteins, DNA, and smaller metabolites.[2-10]

In this regard, three major classes of **NAD**$^+$-consuming enzymes are commonly identified, including sirtuins, (ADP-ribose)polymerases and cyclic ADP-ribose synthases[2-11] Malfunction or dysregulation of these enzymes have been found to disrupt cellular **NAD**$^+$ homoeostasis and, as a consequence, could cause severe diseases, such as cancer, diabetics, atherosclerosis, Alzheimer's disease, depressions, and neurodegeneration.[2-10, 12]

To restore cellular **NAD**$^+$ levels and thus counteract detrimental pathways, inhibition of **NAD**$^+$-consuming enzymes, most notably poly(ADP-ribose)polymerase 1 (PARP1) and CD38/CD157, has shown promise.[13-18] The significance of **NAD**$^+$-mediated processes necessitates the development of new tools and probes to facilitate biophysical analyses and the fabrication of effective discovery assays. Radioactive,[19] clickable,[20, 21] isotopically labeled,[22] and fluorescent[23, 24] **NAD**$^+$ surrogates have been developed. Design of the latter has employed the incorporation of emissive adenosine analogues, including the perturbing 1,N^6-ethenoadenosine and 8-(pyrrol-2-yl)adenosine.[23, 24] To exploit the safety and sensitivity of fluorescence-based tools, which closely reflect the native system, both isomorphicity and isofunctionality of a synthetic analogue must be attained by reducing structural and functional perturbations, respectively, thus ensuring maximum biological compatibility. Concurrently, photophysical responsiveness towards environmental and structural changes is required to enable real-time spectroscopic monitoring.[25]

In the last few years, a new generation of emissive nucleoside analogues has been developed based on a new set of purine-mimicking scaffolds: thieno[3,4-*d*]pyrimidines[26] and isothiazolo[4,3-*d*]pyrimidines.[27] Such isomorphic analogues open a spectral window into processes involving nucleosides and nucleotides derivatives, which is otherwise inaccessible with the native counterparts.[28, 29] A redshifted absorption and useful fluorescence features in the visible range, which are non-existent for the native counterparts, facilitate the fabrication of biochemical and discovery assays with minimal spectral interference by the native chromophores.[28, 29]

Although the thieno[3,4-*d*]pyrimidine family of nucleosides displays outstanding emission features, the isothiazolo[4,3-*d*]pyrimidine-based analogues, albeit somewhat less emissive, provide enhanced isomorphicity and isofunctionality.[30, 31] Having access to both purine analogues, offers, however, a unique opportunity to assess biomolecular recognition features using sensitive fluorescence-based tools. Comparing the native **NAD**$^+$ to its emissive analogues, **NthAD**$^+$, and its singlesite mutant **N^{tz}AD**$^+$ (Figure 1), can provide mechanistic insight into the biomolecular contacts mediated by the imidazole ring, and particularly its N7 nitrogen. Although the purine N7 moiety is known to be crucial for a variety of

biological recognition events, including enzyme-substrate binding (e.g., adenosine–adenosine deaminase),[32] Hoogsteen base pairing,[33] and G-quadruplex formation,[34] its significance in **NAD**$^+$-dependent processes is poorly explored and largely limited to crystallographic studies.[35-39] Unlike N7-deaza-NAD$^+$, which has been employed as an N7-lacking substrate, we hypothesized that **NthAD**$^+$ will likely be emissive and responsive, and thus will likely facilitate fluorescence spectroscopic monitoring of enzymatic activities in real time.[37-40] Furthermore, its redshifted absorption spectra, compared to the native NAD$^+$, facilitate selective excitation and opens a spectral window that is unavailable for the native cofactor. Herein, we therefore describe the synthesis and photophysics of **NthAD**$^+$ (Figure 1), an **NAD**$^+$ analogue containing the isomorphic and highly emissive thieno[3,4-*d*]pyrimidine core. We report its enzymatic synthesis by NMNAT1, and its responsiveness to ADH-mediated reduction to **NthADH**, NADase-catalyzed hydrolysis yielding thADP-ribose (**thADPr**) and consumption by (ADP-ribosyl)ating enzymes including Cholera toxin A and PARP1. Comparison with both the native **NAD**$^+$ and emissive **N^{tz}AD**$^+$ provides insight into its putative recognition features via the basic N7 within the purine skeleton.

Results and Discussion

Synthesis

The preparation of **NthAD**$^+$ was accomplished in two steps starting from the previously synthesized **thA.**[26] The corresponding triphosphate was first chemically synthetized and then enzymatically reacted with β-nicotinamide mononucleotide (NMN) using recombinant nicotinamide mononucleotide adenylyl-transferase1 (NMNAT1).[26] This overcomes the final phosphodiester bond formation in the non-enzymatic syntheses of NAD$^+$ analogues, which is commonly accomplished using coupling reagents (e.g., Staab's reagent) and is associated by long reaction times and low yields.[30] The optimized enzymatic approach can be adapted to preparative scales.[31]

Practically, **thA** was first treated with $POCl_3$ and trimethyl phosphate, followed by the addition of tris(tetrabutylammonium) hydrogen pyrophosphate and tributylamine to yield **thATP** (Scheme 1).[41] It was then treated with β-nicotinamide mononucleotide (NMN) and NMNAT1 (Tris, pH 7.8, 37°C). Addition of inorganic pyrophosphatase (PPase) was required to avoid product inhibition of NMNAT1 by the released pyrophosphate. As assessed by HPLC, quantitative conversion was achieved after 2.5 h and a good isolated yield (81%) was obtained on a 1 mg scale.

Photophysical features

To assess the basic photophysical features of **NthAD**$^+$, its absorption and emission spectra were recorded and compared to the native cofactor and the previously synthesized **N^{tz}AD**$^+$ (Table 1). In comparison to **NAD**$^+$ (λ_{abs} = 259 nm) and similarly to **N^{tz}AD**$^+$ (λ_{abs} = 338 nm), **NthAD**$^+$ features a bathochromically shifted absorption maximum at λ_{abs} = 341 nm (Table 1). Notably, excitation near the absorption maximum was found to cause photo bleaching, which can be avoided by excitation at λ_{ex} = 360 nm, yielding a well-defined emission band with a maximum at 431 nm. Compared to **N^{tz}AD**$^+$ (Φ = 0.044), and as initially hypothesized, **NthAD**$^+$ exhibited a higher quantum yield of Φ = 0.071.

NMNAT1- and ADH-mediated conversion

To evaluate the compatibility of **$N^{th}AD^+$**, and gain access to **$N^{th}ADH$**, its reduction equivalent, a sequential enzymatic conversion assay employing both *Homo sapiens* recombinant NMNAT1 and *Saccharomyces cerevisiae* alcohol dehydrogenase (ADH) was performed.[31, 42] While NMNAT1 naturally accomplishes phosphodiester bond formation between NMN and **ATP** to generate **NAD^+**,[43] ADH reduces **NAD^+** to **NADH** by oxidizing ethanol to acetaldehyde (Scheme 2).

To compare the performance of **^{th}ATP**, **^{tz}ATP** and native **ATP**, the conversion of each nucleotide in this coupled enzymatic process was followed by HPLC, real-time spectroscopic monitoring and steady-state emission and absorption spectroscopy. Treatment with NMN and NMNAT1 facilitated quantitative conversion of both **ATP** and **^{tz}ATP** within 30 min and complete consumption of **^{th}ATP** within 100 min as assessed by HPLC (Figure 2a-c). Spectroscopic assessment highlighted the differences between the analogues. Although the emission intensity decreased upon formation of both **$N^{tz}AD^+$** and **$N^{th}AD$**, it remained unchanged during the formation of “fluorescently silent” **NAD^+** (Figure 2d-f). Notably, all substrates were reduced rapidly within a few minutes in the presence of ethanol and ADH. Spectroscopically, reduction of native **NAD^+** shows an increase in emission intensity, whereas decreasing emission intensity was observed upon reduction of both **^{tz}A**- and **^{th}A**- based synthetic emissive cofactors. Steady-state spectra recorded before treatment and after each enzymatic conversion (Figures 2g-i) reveal phosphodiester bond formation to have little or no effect on the absorption spectra of neither substrate but show a diminished fluorescence for both synthetic cofactors. In all cases, ADH-mediated cofactor reduction results into an increased optical density between 300 and 400 nm, accompanied by a further decrease in emission. This two-step decrease, however, is found to be distinct for each emissive cofactor. Although the initial emission level of **^{th}ATP** is diminished by 70% upon **$N^{th}AD^+$** formation, ADH-mediated reduction causes an additional decrease of only 8%. In contrast, the conversion of **^{tz}ATP** shows a diminution of 40% after the first and 30% after the second reaction.

The enhanced photophysical features of the thieno-based cofactor reveal **$N^{th}AD^+$** to be a suited fluorophore for real-time spectroscopic monitoring of NAD^+ synthesis and reduction processes. Its high photophysical responsiveness may be attributed to intramolecular ground and excited state interactions between the modified purine surrogate and the nicotinamide moiety, interactions that have been evoked for the native cofactor but remain insufficiently explored.[30, 44] The relatively slow conversion of **^{th}ATP** by NMNAT1 suggests **^{th}A** to be less compatible than both the native adenosine and its isothiazolo-based purine analogue. Therefore, we suggest that the imidazole ring and especially contacts through its N7 nitrogen are of significance for NMNAT1-substrate recognition, although the exact contribution of the N7 nitrogen has not been studied in great detail and remains somewhat elusive.[45]

NADase-mediated hydrolysis

To take advantage of the intramolecular photophysical interaction between the nicotineamide moiety and the emissive purine surrogate and to evaluate enzymatic cleavage

of **NthAD$^+$**, an NADase-based assay was applied.[30] This hydrolase catalyzes the glycosidic cleavage of the nicotinamide moiety and the release of ADP-ribose (**ADPr**, Scheme 3), which naturally serves as a secondary messenger and is involved in intramolecular calcium signaling.[46]

Both emissive cofactors were treated with porcine brain NADase. Quantitative conversion was observed after 30 min for **N^{tz}AD$^+$** and 120 min for **NthAD$^+$**, and was accompanied by the formation of **^{tz}ADPr** and **thADPr**, respectively (Figures 3a,b). Assuming similar extinction coefficients for the starting materials and products, **^{tz}ADPr** was obtained in a 2.8-fold higher amount compared to **thADPr**. The latter was isolated, identified and characterized by steady state spectroscopy to reveal bathochromically shifted absorption and emission maxima (λ_{abs} = 340 nm, λ_{em} = 431 nm; Figure S1, Supporting Information). Real-time spectroscopic monitoring of **N^{tz}AD$^+$** hydrolysis showed an increasing emission signal within 25 min (Figure 3c). In contrast, a four-time longer period was required for quantitative **NthAD$^+$** hydrolysis (Figure 3d). The corresponding steady state spectra reveal enhanced optical density and emission intensity within the visible range (Figures 3e,f), in which treatment of **N^{tz}AD$^+$** and **NthAD$^+$** with NADase yielded a 40 and 160% enhancement, respectively, upon enzymatic hydrolysis.

The findings presented above reveal **NthAD$^+$** to be highly photophysically responsive towards glycosidic cleavage and the associated enhanced emission supports the nicotinamide-mediated quenching effects. The comparatively slow hydrolysis of **NthAD$^+$** compared to **N^{tz}AD$^+$** indicates, however, somewhat reduced substrate compatibility for NADase and, as before, suggests the purine N7 moiety to be involved in enzyme-substrate interactions in this enzymatic pocket.

CTA-mediated mono(ADP-ribosyl)ation

To further explore the compatibility of the emissive **NthAD$^+$** and gain insight into more complex and challenging modification processes, enzymatic conversions by the cholera toxin were examined. As a hexameric protein complex, this *Vibrio cholerae* toxin consists of five receptor-binding B subunits (CTB) and an enzymatically active A subunit (CTA).[47] The latter catalyzes the glycosidic cleavage of NAD$^+$ and formation of ADP-ribose (**ADPr**), which can be transferred onto arginine (Arg) side chains and other guanidine-containing derivatives.[48] This process, known as mono(ADP-ribosyl)ation, classifies CTA as a mono(ADP-ribosyl)transferase. Furthermore, CTA is found to modify and intrinsically inhibit the guanine nucleotide-binding G_S alpha subunit ($G_{\alpha S}$) of heterotrimeric G_S Proteins, which causes severe dehydration and other cholera-associated symptoms.[49]

Although Arg-containing proteins serve as major intracellular CTA targets, the less bulky and easily detectable agmatine (Agm), is commonly employed as an Arg surrogate for CTA-based in vitro assays.[50] By utilizing this approach, we have recently found CTA to consume **N^{tz}AD$^+$** and form mono(^{tz}ADP-ribosyl)ated agmatine (**^{tz}ADPr-Agm**, Scheme 4). To compare the suitability of **NthAD$^+$**, solutions of the cofactors and Agm were treated with CTA. This cost-intensive assay and small reaction volumes, however, disfavored real-time spectroscopic monitoring and necessitated sequential records of steady state spectra.

Samples were thus taken after 0, 20, 50, 90, and 180 min and analyzed both spectroscopically and by HPLC. Conversion of native NAD^+ was exclusively monitored by HPLC.

Upon treatment with CTA, quantitative conversion was detected by HPCL after 90 min for **NAD^+** and 180 min for both **$N^{tz}AD^+$** and **$N^{th}AD^+$** (Figures 4a-c). In addition, **thADPr-Agm** was isolated, identified and spectroscopically characterized, revealing bathochromically shifted absorption and emission maxima (λ_{abs} = 341 nm, λ_{em} = 425 nm, Figure S3, Supporting Information). Along with the formation of Agm adducts, hydrolysis to the corresponding **ADPr** analogues was observed as a major side reaction in all three cases. Assuming similar extinction coefficients for the starting materials and Agm adducts, the by-product/product ratios amount to 0.20, 0.37, and 0.59 for the native-, isothiazolo-, and thieno-based cofactors, respectively. Furthermore, treatment of either fluorescent cofactor with CTA causes a significant increase in emission intensity, as assessed by steady state spectroscopy (Figures 4e,f). CTA-mediated conversion of **$N^{th}AD^+$** yielded an emission enhancement of 360%, whereas conversion of **$N^{tz}AD^+$** yielded a 70% increase only.

To compare the chromatographic and spectroscopic monitoring methods, the integrated HPLC product peak areas and emission intensities were plotted against time. The HPLC-derived plots reveal a faster formation of **ADPr-Agm** compared to both **^{tz}ADPr-Agm** and **thADPr-Agm**, of which the latter is the slowest to form (Figure 4d, solid lines). The normalized emission intensities (Figure 4d, dashed lines) confirm the kinetics observed for **$N^{th}AD^+$** conversion but suggest **$N^{tz}AD^+$** to convert slightly slower than indicated by HPLC. The slight deviation between spectroscopically and HPLC-derived kinetic measurements has been seen before[30] and could be attributed to the formation of by- or decomposition products, which affect the overall emission intensity. Despite these minor limitations, **$N^{th}AD^+$** can be used as a powerful fluorophore due to its high spectroscopic responsiveness upon mono(thADP-ribosyl)ation. Its slow conversion, as well as the excessive formation of **thADPr**, reveal, however, a poorer recognition by CTA compared to both **$N^{th}AD^+$** and **NAD^+**. These findings further support substrate recognition through the purine N7 nitrogen. Although X-ray-based studies of Fieldhouse et al. have revealed multiple intermolecular interactions between **NAD^+** and CTA in detail, the involvement of the N7 nitrogen has remained crystallographically elusive.[36]

PARP1-mediated poly(ADP-ribosyl)ation

In contrast to CTA, which acts as a mono(ADP-ribose)transferase, PARP1 mediates poly(ADP-ribosyl)ation by transferring multiple **ADPr** units to itself or other target proteins, forming poly(ADP-ribose) linkages (**pADPr**, Scheme 5). Depending on its chain structure and length, such posttranslational modifications can affect the activity and localization of associated proteins and their non-covalent interaction with other binding partners.[51] Hence, PARP1 functions as a regulatory key enzyme, which is involved in DNA damage response, metabolic regulation and transcriptional activation processes, among others.[52] Association with severe diseases makes PARP1 an attractive therapeutic target, which is driving the development of new inhibitors and treatment of breast, prostate, and ovarian cancer, among others.[13-17]

Given that PARP1 can act as both the enzyme and the target, we studied its auto-poly(ADP-ribosyl)ation using all cofactors and calf thymus DNA as the activating agent.[21,53,54] Accordingly, a solution of PARP1 was treated with calf thymus DNA before inducing the reaction with **N^{tz}AD^{+}** or **NthAD^{+}**. Positive controls included native **NAD^{+}** and negative controls included reaction mixtures without the cofactors. The conversion was then monitored at different time points both spectroscopically and by sodium dodecyl sulfate polyacrylamide gel electrophoresis (SDS-PAGE). To facilitate adequate detection and differentiation between modified and unmodified PARP1, western blotting based on anti-PARP1 and anti-pADPr antibodies was performed.[21]

Initial attempts to spectroscopically monitor this transformation in real time did not reveal any change in emission intensity, neither upon treatment with **N^{tz}AD^{+}** nor with **NthAD^{+}**. The Coomassie-stained SDS-PAGE (Figure 5a) did show, however, PARP1-related bands to decrease in intensity over time for both cofactors. This decrease is most striking upon adding **NAD^{+}** and still substantial upon **N^{tz}AD^{+}** treatment, whereas addition of **NthAD^{+}** shows only little effect. Modified PARP1, in contrast, remains undetectable by Coomassie staining and necessitated western blotting for further analysis. The respective blot (Figure 5b) confirms a diminishing concentration of unmodified PARP1 (green channel) upon addition of **NAD^{+}** or **N^{tz}AD^{+}**, respectively. Visualization of anti-pADPr (blue channel) confirms the formation of **pADPr**- and **p^{tz}ADPr**-modified PARP1, respectively, which is manifested in smeared higher MW bands. **NAD^{+}**-induced formation of auto-modified PARP1 is detected as early as after 2 min and found to increase for 60 min. A reduced amount of **pADPR**-modified PARP1 was detected after 180 min. In comparison, **p^{tz}ADPr**-related bands arise at lower MW, are less intense and show a regression already after 10 min. In contrast, no **pthADPr** was detected upon treatment with **NthAD^{+}**.

An important consideration, when assessing the observations articulated above, is the biochemical specificity of the antibodies, particularly the anti-pADPr one. Designed to bind native **pADPr**, anti-pADPr is known to interact with 3–4 **ADPr** units of linear **pADPr**, which can be associated with proteins both covalently and non-covalently.[55, 56] Oligomers consisting of ten **ADPr** units or less are not efficiently captured, whereas polymers of > 20 **ADPr** units facilitate proper binding, as revealed by competitive binding assays.[55] Beside these known limitations, neither the exact epitopes of anti-pADPr nor its interaction with **p^{tz}ADPr** or **pthADPr** are known.[57] Hence, a reduced or even no affinity of anti-pADPr towards synthetic **pADPr** analogues cannot be excluded, but will be neglected in the following evaluation.

To further analyze the observations discussed above, two opposite and kinetically divergent processes must be considered. Firstly, the increasing amount of modified PARP1 and the shift to higher MW reveal an ongoing polymerization reaction upon treatment with **NAD^{+}** and **N^{tz}AD^{+}**. Secondly, the subsequent regression of modified PARP1 indicates decomposition and cleavage of the **pADPr**-protein linkages, which are known to be fragile ($t_{1/2}$ < 1 h, pH 7.5).[58, 59] Notably, this decomposition process is favored in the presence of nicotinamide, which is released upon poly(ADP-ribosyl)ation. Previous studies under similar conditions (pH 8.0, 20 μg rat liver PARP, 100 nM **NAD^{+}**, 23°C) showed a regressing amount of **pADPr**-modified PARP after 50 min, which is consistent with the kinetics

obtained for **NAD**$^+$-induced PARP1 auto-modification.[59] The lower amount of **p^{tz}ADPr** and premature regression of the correspondingly modified PARP1 suggest reduced compatibility, which could reflect less effective oligomerization or faster degradation of the shorter oligomers formed. Alternatively, the apparent absence of **pthADPr**-modified PARP1 suggests poly(thADP-ribosyl)ation to be severely limited with **NthAD**$^+$, if not impossible, and illustrates its diminished recognition as a PARP1 substrate. This is supported by crystallographic studies of **NAD**$^+$-bound PARP1, which illustrate hydrophobic interactions between isoleucine (Ile872) and the adenosine imidazole ring. Additionally, the purines N7 nitrogen is proposed to interact with the protein through an aspartic acid residue.[35] Such enzyme-substrate interactions, although possible with **N^{tz}AD**$^+$, cannot be accommodated by **NthAD**$^+$, the thiopheno-based system lacking a basic N at the corresponding position.

Conclusion

This study set out to prepare **NthAD**$^+$, an N7-lacking, thieno[3,4-*d*]pyrimidine-based **NAD**$^+$ surrogate, and assess its utility for monitoring **NAD**$^+$-dependent reactions by spectroscopic means. To this end, we employed recombinant NMNAT1 that facilitates the preparative scale synthesis of **NthAD**$^+$ from the emissive **thATP**. When compared to our previously developed analogue **N^{tz}AD**$^+$ (λ_{abs} = 338 nm, λ_{em} = 411 nm, Φ = 0.044), **NthAD**$^+$ showed improved photophysical features including red-shifted absorption and emission maxima (λ_{abs} = 341 nm, λ_{em} = 431 nm) and a higher emission quantum yield (Φ = 0.071). Moreover, **NthAD**$^+$ served as a viable substrate for ADH-mediated reduction affording **NthADH**, NADase-catalyzed hydrolysis yielding **thADPr** and CTA-mediated mono(ADP-ribosyl)ation. Photophysical analysis revealed **NthAD**$^+$ to be substantially more responsive towards enzymatic conversions than its isothiazolo-based analogue, and thus suited as a fluorescent probe for their spectroscopic real-time monitoring. Spectroscopic and HPLC-based analyses found **NthAD**$^+$ to be less isofunctional than both **NAD**$^+$ and **N^{tz}AD**$^+$, which is manifested in lower conversion rates or increased by-product formation. When assessing PARP1-mediated auto-poly(ADP-ribosyl)ation, no conversion was observed upon treatment with **NthAD**$^+$ at all, whereas **N^{tz}AD**$^+$ was converted successfully, although only to a lower extent compared to its native cofactor, indicating an inherent PARP1-N7 dependency. These studies demonstrate the utility of both **N^{tz}AD**$^+$ and **NthAD**$^+$, particularly when used side by side, for investigating biomolecular recognition features that involve purine N7 interactions. Even though being quenched within pADPr, both emissive analogues can be easily employed to monitor enzymatic reactions including NAD$^+$ formation, oxidation/reduction, hydrolysis, and, potentially, mono(ADP-ribosyl)ation in real time.

Experimental Section

Synthesis of thATP

A suspension of **thA** (50 mg, 0.18 mmol, 1.0 equiv) in trimethyl phosphate (TMP; 1.8 mL) was treated with $POCl_3$ (41 μL, 0.44 mmol, 2.5 equiv) at 0°C under stirring. After 1 h stirring at 0°C, additional $POCl_3$ (41 μL, 0.44 mmol, 2.5 equiv) was added and the suspension was stirred at 0 °C for another 2 h. After treatment with tris(tetrabutylammonium) hydrogen pyrophosphate (164 mg, 0.88 mmol, 5.0 equiv)

dissolved in dry DMF (1.8 mL), tributyl amine (0.21 mL, 0.88 mmol, 5.0 equiv) was added dropwise and the reaction mixture was stirred at 0 °C for 2 h. The reaction mixture was quenched with ice-cold 0.05 M tetraethylammonium bromide (TEAB; 5. 0 mL), stirred at 0°C for 15 min and washed with EtOAc (10 mL). After extracting the organic phase with 0.05 M TEAB (3×5 mL), the aqueous phases were combined and concentrated in vacuo. The crude product was purified by ion exchange chromatography (Sephadex DEAE A25 column; 0.05 M 0.5 M TEAB; 4°C). After concentration in vacuo and lyophilization, the resulting solid was dissolved in ddH_2O (1.00 mL) and purified by HPLC (70 μL injections, method see Supporting Information). Lyophilization of the collected fraction afforded a white solid of **thATP** (0.011 mmol, 6.1%), which was used without further purification. ^{1}H NMR (300 MHz, D_2O): δ=8.55 (s, 1H), 8.22 (s, 1H), 5.44 (d, J=7.43 Hz, 1H), 4.42 (dd, J= 5.10, 3.11 Hz, 1H), 4.35 (dd, J=7.43, 5.10 Hz, 1H), 4.30 (m, 1H), 4.22 ppm(m, 2H); ^{31}P NMR (202 MHz, D_2O): δ=−9.92 (d, J=20.0 Hz), −10.83 (d, J=19.5 Hz), −22.57 ppm (m); HRMS (ESI): *m/z* calcd for [$C_{11}H_{16}N_3O_{13}P_3S$-$H^+$]: 521.9544 [$M$–H]$^-$; found 521.9536.

Synthesis of NthAD

A solution of Tris (50 mM), KCl (50 mM), NaCl (50 mM), $MgCl_2$ (12 m_m), **thATP** (1.5 mM), NMN (2.0 mM) and PPase (10 U) in ddH_2O (1.50 mL) was left for equilibration at 37°C for 5 min. After addition of NMNAT1 (Novus Biologicals, 0.42 U[60]), the reaction mixture was gently mixed and left for 2.5 h at 37 °C. The reaction was monitored by HPCL (method see Supporting Information) and stopped by freezing the mixture at −78°C. The reaction mixture was concentrated to a volume of 0.3 mL by lyophilization. Purification by HPLC (100 μL injections, method see Supporting Information) and subsequent lyophilization afforded a white solid of **NthAD** (1.82 mM, 81%). ^{1}H NMR (300 MHz, D_2O): δ=9.30 (s, 1H), 9.10 (d, J=6.19 Hz, 1H), 8.76 (d, J=8.20 Hz, 1H), 8.28 (s, 1H), 8.14 (dd, J=7.89, 6.46 Hz, 1H), 8.00 (s, 1H), 4.53 (d, J=2.48 Hz, 1H), 4.46 (t, J=5.23 Hz, 1H), 4.41 (m, 2H), 4.36 (m, 2H), 4.26 (m, 1H), 4.21 (m, 1H), 4.14 ppm (m, 1H); ^{31}P NMR (202 MHz, D_2O): δ= −10.63 (d, J=18.73 Hz), −11.07 ppm (d, J=19.91 Hz); HRMS (ESI): *m/z* calcd for [$C_{22}H_{29}N_5O_{14}P_2S$–$H^+$]: 678.0678 [M-H]$^-$; found 678.0679.

Steady-state absorption and emission spectroscopy

Steady state absorption spectra were measured on a Shimadzu UV-2450 spectrophotometer setting the slit at 1 nm and using a resolution of 0.5 nm. Steady state emission spectra were measured on a Horiba Fluoromax-4 setting both the excitation and the emission slits at 3 nm, the resolution at 1 nm and the integration time at 0.1 s. Both instruments were equipped with a thermostat-controlled ethylene-glycol-water bath fitted to specially designed cuvette holders and the temperature was kept at 25.0±0.1 °C or 37.0±0.1 °C, respectively. Native, **^{tz}A**-, and **thA**-based probes were excited at 335, 330, and 360 nm, respectively. All spectra were corrected for the blank. Further assay-dependent specificities can be found in the Supporting Information.

Spectroscopic real-time monitoring

Enzymatic conversion was followed by monitoring the emission intensity at a fixed wavelength as function of time. Emission was measured on a Horiba Fluoromax-4 equipped

with a cuvette holder with a built-in stirring system, setting both the excitation and emission slits at 3 nm and taking a point at regular time intervals. The temperature was kept at 25.0±0.1 °C or 37.0±0.1 °C, respectively. Emission was monitored at 410 nm (λ_{ex} = 360 nm), 410 nm (λ_{ex} = 330 nm) and 465 nm (λ_{ex} = 335 nm) for **thATP**, **^{tz}ATP**, and **ATP**, respectively. Further assay-dependent specificities can be found in the Supporting Information.

NMNAT1- and ADH-mediated conversion

In a 125 μL cuvette, buffer containing Tris-HCl (50 mM, pH 7.8), NaCl (50 mM), KCl (50 mM), $MgCl_2$ (12 mM), NMN (15 μM), PPase (0.3 U), EtOH (17 μM), and **thATP**, **^{tz}ATP**, or **ATP** (15 μM) was added to set up a total reaction volume of 500 μL. The solution was left to stabilize at 37.0±0.1 °C for 30 minutes before NMNAT1 (14 mU) was added. The mixture was promptly mixed and left at 37.0±0.1 °C for 6000 s (**thATP**) or 1800 s (**^{tz}ATP, ATP**), respectively. To start the second reaction, the mixture was treated with ADH (5 μL, 58 U/μM substrate), promptly mixed, and left at 37.0±0.1 °C for 600 s (**thATP**) or 300 s (**^{tz}ATP, ATP**). All reactions were performed in duplicates.

NADase-mediated hydrolysis

In a 3 mL cuvette equipped with a stirring bar, buffer containing Tris-HCl (50 mM, pH 7.8), NaCl (50 mM), KCl (50 mM), and **NthAD$^+$** or **N^{tz}AD$^+$** (7.5 μM) was added to set up a final reaction volume of 3 mL. The solution was left to stabilize at 25.0±0.1 °C for 30 min before an aliquot of suspended NADase (30 mU) was added. The suspension was promptly mixed and left at 25.0±0.1 °C for 6300 s (**NthAD$^+$**) or 1500 s (**N^{tz}AD$^+$**). All reactions were performed in duplicates.

CTA-mediated mono(ADP-ribosyl)ation

In a 600 μL sterilized conical vial, buffer containing potassium phosphate (pH 7.2; 160 mM), dithiothreitol (DTT; 20 mM), agmatine sulfate (15 mM), $MgCl_2$ (20 mM), ovalbumine (4 gL^{-1}) and **NAD$^+$**, **NthAD$^+$** or **N^{tz}AD$^+$** (7.5 μM) was added to set up a final reaction volume of 25.5 μL. The solution was left to stir at 25.0±0.1 °C for 5 minutes to equilibrate. To start the reaction, CTA (255 μg) was added. All reactions were performed in duplicates.

PARP1-mediated poly(ADP-ribosyl)ation

In a 600 μL sterilized conical vial, 4× buffer (30 μL) containing (Tris-HCl pH 8.0, 400 mM), $MgCl_2$ (40 mM), DTT (4 mM) and calf thymus DNA (15 mgL^{-1}) was added and left to stabilize at 37°C for 3 min. Subsequently, PARP1 (4.1 μL, 150 nM final concn) was added, the solution was gently mixed and left at 37°C for another 3 min to activate PARP1. After treatment with **NthAD$^+$**, **N^{tz}AD$^+$**, or **NAD$^+$** (60 μL, 500 μM final concn), the mixture was gently mixed and left at 37 °C for 180 min. All reactions were performed in duplicates.

SDS-PAGE

For sodium dodecyl sulfate polyacrylamide gel electrophoresis (SDS-PAGE), samples of 9 μL were taken after given time points. The reaction was stopped by treating the samples with 4× loading buffer and subsequent heating at 95°C for 5 min. In order to avoid decomposition

of modified PARP1, samples were immediately frozen at −78°C and stored at −20°C. Prior resolution, reaction samples were thawed and loaded onto 8.0% SDS gels according to Laemmli's protocol.[61] Electrophoresis was performed at 100 V for 30 min, then 150 V for 30 min, and 200 V for 60 min in SDS running buffer.

Coomassie staining

After resolving the reaction mixtures by SDS-PAGE, the gel was rinsed in ddH_2O once, immersed in staining solution (0.15% Coomassie Brilliant Blue R-250, 45% MeOH, 10% acetic acid in ddH_2O), microwaved for 50 s and shaken for 20 min at RT. After rinsing with ddH_2O, the gel was covered with destaining solution (5.0% MeOH, 7.5% acetic acid in ddH_2O), microwaved for 50 s and shaken for 24 h at RT. The destaining solution was replaced frequently. To estimate molecular weights, PageRuler Plus Prestained Protein Ladder (Thermo Fisher) was used as a reference.

Western blot

After resolving the reaction mixtures by SDS-PAGE, gels were electrophoretically transferred onto a PVDF membrane (GE HealthCare) in 1 × NuPAGE Transfer Buffer (ThermoFisher) + 10% MeOH at 30 V for 70 min. The membrane was blocked in Odyssey Blocking Buffer (LI-COR) at RT for 30 min under agitation. After blocking, the membrane was incubated with anti-PAR [10H] antibody (Tulip BioLabs, 10 $\mu g mL^{-1}$) in 1×TBST buffer at 4°C overnight. The membrane was washed three times with 1 × TBST buffer for 5 min each and incubated with anti-mouse IRDye 680RD antibody (LI-COR, diluted 1:15 000) at RT for 1 h. Subsequently, the membrane was washed three times with 1×TBST buffer + 0.2% SDS for 5 min each and then three times with 1×PBS-buffer for 5 min each. The membrane was incubated with anti-PARP1 antibody (Tulip BioLabs, 1 $\mu g mL^{-1}$) in 1×TBST buffer at RT for 1 h. The membrane was washed three times with 1×TBST buffer for 5 min each and incubated with anti-chicken secondary antibody (diluted 1:15000) at RT for 1 h. Subsequently, the membrane was washed three times with 1×TBST buffer + 0.2% SDS for 5 min each and then three times with 1×PBS buffer for 5 min each. Finally, the membrane was stored in PBS buffer until imaged and quantitatively analyzed via Image Studio (LI-COR).

Supplementary Material

Refer to Web version on PubMed Central for supplementary material.

Acknowledgements

We thank the National Institutes of Health for generous support (GM 069773) and UCSD Chemistry & Biochemistry MS Facility. We are grateful to Dr. Alexander Rovira for helpful discussions and to the DAAD and Bavarian State for supporting J.F. with the PROSA LMU scholarship.

References

[1]. Sellés Vidal L, Kelly CL, Mordaka PM, Heap JT, Biochim. Biophys. Acta 2018, 1866, 327.

[2]. Houtkooper RH, Canto C, Wanders RJ, Auwerx J, Endocr. Rev 2010, 31, 194. [PubMed: 20007326]

[3]. Cohen MS, Chang P, Nat. Chem. Biol 2018, 14, 236. [PubMed: 29443986]

[4]. Current Topics in Microbiology and Immunology, *Vol.* 384 (Ed.: Koch-Nolte F), Springer International Publishing, Cham, 2015.

[5]. Lüscher B, Bütepage M, Eckei L, Krieg S, Verheugd P, Shilton BH, Chem. Rev 2018, 118, 1092. [PubMed: 29172462]

[6]. Palazzo L, Mikoč A, Ahel I, FEBS J. 2017, 284, 2932. [PubMed: 28383827]

[7]. Schreiber V, Dantzer F, Ame J-C, de Murcia G, Nat. Rev. Mol. Cell Biol 2006, 7, 517. [PubMed: 16829982]

[8]. Lin H, Org. Biomol. Chem 2007, 5, 2541. [PubMed: 18019526]

[9]. Barkauskaite E, Jankevicius G, Ahel I, Mol. Cell 2015, 58, 935. [PubMed: 26091342]

[10]. Michan S, Sinclair D, Biochem. J 2007, 404, 1. [PubMed: 17447894]

[11] a). Chambon P, Weill JD, Mandel P, Biochem. Biophys. Res. Commun 1963, 11, 39; [PubMed: 14019961] b)De Flora A, Zocchi E, Guida L, Franco L, Bruzzone S, Ann. N. Y. Acad. Sci 2004, 1028, 176; [PubMed: 15650244] c)Imai S, Armstrong CM, Kaeberlein M, Guarente L, Nature 2000, 403, 795. [PubMed: 10693811]

[12] a). Cantó C, Menzies KJ, Auwerx J, Cell Metab. 2015, 22, 31; [PubMed: 26118927] b)Elhassan YS, Philp AA, Lavery GG, J. Endocr. Soc 2017, 1, 816; [PubMed: 29264533] c)Verdin E, Science 2015, 350, 1208; [PubMed: 26785480] d)Fang EF, Lautrup S, Hou Y, Demarest TG, Croteau DL, Mattson MP, Bohr VA, Trends Mol. Med 2017, 23, 899; [PubMed: 28899755] e)Haigis MC, Sinclair DA, Annu. Rev. Pathol. Mech. Dis 2010, 5, 253;f)Belenky P, Bogan KL, Brenner C, Trends Biochem. Sci 2007, 32, 12; [PubMed: 17161604] g)Houtkooper RH, Pirinen E, Auwerx J, Nat. Rev. Mol. Cell Biol 2012, 13, 225 EP. [PubMed: 22395773]

[13]. Malyuchenko NV, Kotova EY, Kulaeva OI, Kirpichnikov MP, Studitskiy VM, Acta Naturae 2015, 7, 27. [PubMed: 26483957]

[14]. Dziadkowiec KN, Gąsiorowska E, Nowak-Markwitz E, Jankowska A, Menopause Rev. 2016, 4, 215.

[15]. Curtin NJ, Szabo C, Mol. Aspects Med 2013, 34, 1217. [PubMed: 23370117]

[16]. Drenichev MS, Mikhailov SN, Bioorg. Med. Chem. Lett 2016, 26, 3395. [PubMed: 27318540]

[17]. Wahlberg E, Karlberg T, Kouznetsova E, Markova N, Macchiarulo A, Thorsell A-G, Pol E, Frostell A, Ekblad T, Öncü D, Kull B, Robertson GM, Pellicciari R, Schüler H, Weigelt J, Nat. Biotechnol 2012, 30, 283. [PubMed: 22343925]

[18] a). Kwong AKY, Chen Z, Zhang H, Leung FP, Lam CMC, Ting KY, Zhang L, Hao Q, Zhang L-H, Lee HC, Biochemistry 2012, 51, 555; [PubMed: 22142305] b)Lokhorst HM, Plesner T, Laubach JP, Nahi H, Gimsing P, Hansson M, Minnema MC, Lassen U, Krejcik J, Palumbo A, van de Donk NWCJ, Ahmadi T, Khan I, Uhlar CM, Wang J, Sasser AK, Losic N, Lisby S, Basse L, Brun N, Richardson PG, N. Engl. J. Med 2015, 373, 1207; [PubMed: 26308596] c)Virág L, Szabó C, Pharmacol. Rev 2002, 54, 375. [PubMed: 12223530]

[19]. Methods in Enzymology, (Eds.: McCormick DB, Wright LD) *Vol.* 18, *Part B,* Academic Press, New York, 1971.

[20]. Jiang H, Kim JH, Frizzell KM, Kraus WL, Lin H, J. Am. Chem. Soc 2010, 132, 9363. [PubMed: 20560583]

[21]. Wang Y, Rösner D, Grzywa M, Marx A, Angew. Chem. Int. Ed 2014, 53, 8159;Angew. Chem 2014, 126, 8298.

[22]. Evans J, Wang T-C, Heyes MP, Markey SP, Anal. Biochem 2002, 306, 197. [PubMed: 12123656]

[23]. Lee CY, Everse J, Arch. Biochem. Biophys 1973, 157, 83. [PubMed: 4352059]

[24]. Pergolizzi G, Butt JN, Bowater RP, Wagner GK, Chem. Commun 2011, 47, 12655.

[25]. Sinkeldam RW, Tor Y, Org. Biomol. Chem 2007, 5, 2523. [PubMed: 18019524]

[26]. Shin D, Sinkeldam RW, Tor Y, J. Am. Chem. Soc 2011, 133, 14912. [PubMed: 21866967]

[27]. Rovira AR, Fin A, Tor Y, J. Am. Chem. Soc 2015, 137, 14602. [PubMed: 26523462]

[28]. Sinkeldam RW, Greco NJ, Tor Y, Chem. Rev 2010, 110, 2579. [PubMed: 20205430]

[29]. Fluorescent Analogs of Biomolecular Building Blocks. Design and Applications, (Eds.: Wilhelmsson M, Tor Y), Wiley, Hoboken, 2016.

[30]. Rovira AR, Fin A, Tor Y, J. Am. Chem. Soc 2017, 139, 15556. [PubMed: 29043790]

[31]. Hallé F, Fin A, Rovira AR, Tor Y, Angew. Chem. Int. Ed 2018, 57, 1087;Angew. Chem 2018, 130, 1099.

[32] a). Sinkeldam RW, McCoy LS, Shin D, Tor Y, Angew. Chem. Int. Ed 2013, 52, 14026;Angew. Chem 2013, 125, 14276;b)Mizrahi RA, Shin D, Sinkeldam RW, Phelps KJ, Fin A, Tantillo DJ, Tor Y, Beal PA, Angew. Chem. Int. Ed 2015, 54, 8713;Angew. Chem 2015, 127, 8837.

[33]. Nikolova EN, Zhou H, Gottardo FL, Alvey HS, Kimsey IJ, Al-Hashimi HM, Biopolymers 2013, 99, 955. [PubMed: 23818176]

[34]. Burge S, Parkinson GN, Hazel P, Todd AK, Neidle S, Nucleic Acids Res. 2006, 34, 5402. [PubMed: 17012276]

[35]. Ruf A, de Murcia G, Schulz GE, Biochemistry 1998, 37, 3893. [PubMed: 9521710]

[36]. Fieldhouse RJ, Jørgensen R, Lugo MR, Merrill AR, J. Biol. Chem 2012, 287, 21176. [PubMed: 22535961]

[37]. Lennon MB, Joseph W, Suhadolnik RJ, Biochem. Biophys. Res. Commun 1976, 72, 530. [PubMed: 186048]

[38]. Suhadolnik RJ, Lennon MB in Alcohol and Aldehyde Metabolizing Systems, Academic Press, New York, 1977, pp. 123–136.

[39]. Bailey VC, Sethi JK, Fortt SM, Galione A, Potter BVL, Chem. Biol 1997, 4, 51. [PubMed: 9070427]

[40]. Seela F, Zulauf M, Sauer M, Deimel M, Helv. Chim. Acta 2000, 83, 910.

[41]. McCoy LS, Shin D, Tor Y, J. Am. Chem. Soc 2014, 136, 15176. [PubMed: 25255464]

[42]. Balducci E, Emanuelli M, Raffaelli N, Ruggieri S, Amici A, Magni G, Orsomando G, Polzonetti V, Natalini P, Anal. Biochem 1995, 228, 64. [PubMed: 8572289]

[43]. Schweiger M, Hennig K, Lerner F, Niere M, Hirsch-Kauffmann M, Specht T, Weise C, Oei SL, Ziegler M, FEBS Lett. 2001, 492, 95. [PubMed: 11248244]

[44] a). Scott TG, Spencer RD, Leonard NJ, Weber G, J. Am. Chem. Soc 1970, 92, 687;b)Gruber BA, Leonard NJ, Proc. Natl. Acad. Sci. USA 1975, 72, 3966; [PubMed: 172889] c)Hull RV, Conger PS, Hoobler RJ, Biophys. Chem 2001, 90, 9; [PubMed: 11321678] d)Tanaka M, Ohkubo K, Fukuzumi S, J. Phys. Chem. A 2006, 110, 11214. [PubMed: 16986858]

[45] a). Werner E, Ziegler M, Lerner F, Schweiger M, Heinemann U, FEBS Lett. 2002, 516, 239; [PubMed: 11959140] b)Zhou T, Kurnasov O, Tomchick DR, Binns DD, Grishin NV, Marquez VE, Osterman AL, Zhang H, J. Biol. Chem 2002, 277, 13148. [PubMed: 11788603]

[46]. Kim H, Jacobson EL, Jacobson MK, Mol. Cell. Biochem 1994, 138, 237. [PubMed: 7898469]

[47]. Spangler BD, Microbiol. Rev 1992, 56, 622. [PubMed: 1480112]

[48]. Moss J, Vaughan M, Proc. Natl. Acad. Sci. USA 1978, 75, 3621. [PubMed: 211502]

[49] a). a) de Haan L, Hirst TR, Mol. Membr Biol 2004, 21, 77; [PubMed: 15204437] b)Levitzki A, Bar-Sinai A, Pharmacol. Ther 1991, 50, 271. [PubMed: 1754602]

[50]. Glowacki G, Braren R, Firner K, Nissen M, Kühl M, Reche P, Bazan F, Cetkovic-Cvrlje M, Leiter E, Haag F, Koch-Nolte F, Protein Sci. 2009, 11, 1657.

[51]. Gibson BA, Kraus WL, Nat. Rev. Mol. Cell Biol 2012, 13, 411. [PubMed: 22713970]

[52] a). Andrabi SA, Umanah GKE, Chang C, Stevens DA, Karuppagounder SS, Gagne J-P, Poirier GG, Dawson VL, Dawson TM, Proc. Natl. Acad. Sci. USA 2014, 111, 10209; [PubMed: 24987120] b)Hassa PO, Buerki C, Lombardi C, Imhof R, Hottiger MO, J. Biol. Chem 2003, 278, 45145; [PubMed: 12960163] c)Lupo B, Trusolino L, Biochim. Biophys. Acta 2014, 1846, 201; [PubMed: 25026313] d)Piao L, Fujioka K, Nakakido M, Hamamoto R, Front. Biosci 2018, 23, 13;e)Li M, Yu X, Cancer Cell 2013, 23, 693. [PubMed: 23680151]

[53]. Kirsten E, Kun E, Mendeleyev J, Ordahl CP in Epigenetics Protocols, *Vol.* 287 (Ed.: Tollefsbol TO), Humana Press, Inc., Totowa, 2004, p. 137.

[54]. Benjamin RC, Gill DM, J. Biol. Chem 1980, 255, 10502. [PubMed: 6253477]

[55]. Kawamitsu H, Hoshino H, Okada H, Miwa M, Momoi H, Sugimura T, Biochemistry 1984, 23, 3771. [PubMed: 6206890]

[56] a). Fahrer J, Kranaster R, Altmeyer M, Marx A, Bürkle A, Nucleic Acids Res. 2007, 35, e143; [PubMed: 17991682] b)Gagné J-P, Isabelle M, Lo KS, Bourassa S, Hendzel MJ, Dawson VL, Dawson TM, Poirier GG, Nucleic Acids Res. 2008, 36, 6959. [PubMed: 18981049]

[57]. Vivelo CA, Leung AKL, Proteomics 2015, 15, 203. [PubMed: 25263235]

[58] a). Moyle PM, Muir TW, J. Am. Chem. Soc 2010, 132, 15878; [PubMed: 20968292] b)Hassa PO, Haenni SS, Elser M, Hottiger MO, Microbiol. Mol. Biol. Rev 2006, 70, 789. [PubMed: 16959969]

[59]. Bauer PI, Hakam A, Kun E, FEBS Lett. 1986, 195, 331. [PubMed: 2935422]

[60]. 1 unit (U) is the amount of enzyme that catalyzes the reaction of 1 μmol of substrate per minute.

[61]. Laemmli UK, Nature 1970, 227, 680. [PubMed: 5432063]

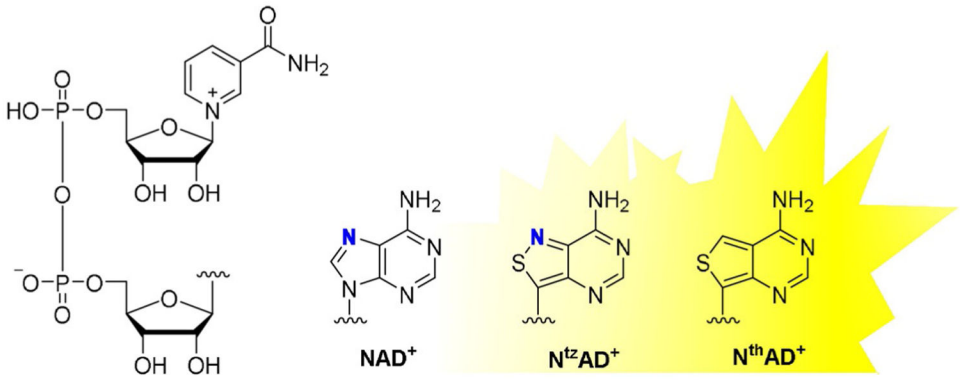

Figure 1.

Structural formula of native **NAD**$^+$ and emissive analogues **N^{tz}AD**$^+$ and **NthAD**$^+$. Purine N7 moieties are highlighted in blue.

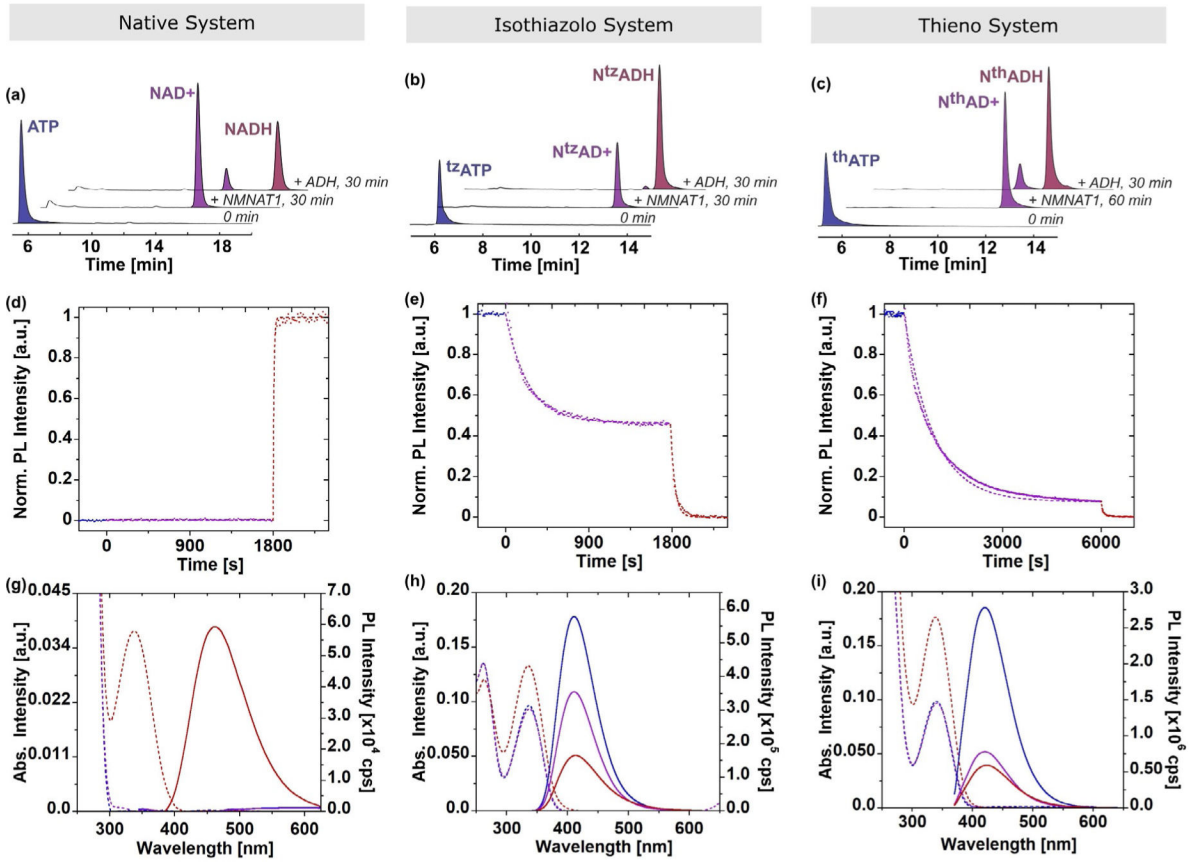

Figure 2.

Monitoring of the NMNAT1-mediated synthesis and ADH-catalyzed reduction of native **NAD**$^+$ and emissive analogues. Top: HPLC traces of (a) *ATP*, (b) ^{tz}**ATP** and (c) th**ATP** (blue each), corresponding **NAD**$^+$ species (purple) and their reduced forms (red) monitored before conversion, 30 min (th**ATP**: 60 min) after treatment with NMNAT1 and 30 min after the addition of ADH at $\boldsymbol{\lambda}_{abs}$ = 260, 330 and 340 nm, respectively. Center: normalized emission intensity signals over time recorded for the conversion of (d) **ATP** at 465 nm (λ_{ex} = 335 nm), (e) ^{tz}**ATP** at 410 nm (λ_{ex} = 330 nm) and (f) th**ATP** at 410 nm (λ_{ex} = 360) before (blue) and upon (purple) treatment with NMNAT1 and after the addition of ADH (red). Bottom: Steady-state absorption (dashed lines) and emission (solid lines) spectra for the conversion of (g) **ATP** (λ_{ex} = 335 nm), (h) ^{tz}**ATP** (λ_{ex} = 330 nm) and (i) th**ATP** (λ_{ex} = 360 nm) recorded before conversion (blue), 30 min (th**ATP**: 60 min) after treatment with NMNAT1 (purple) and 10 min (th**ATP**: 20 min) after the addition of ADH (red).

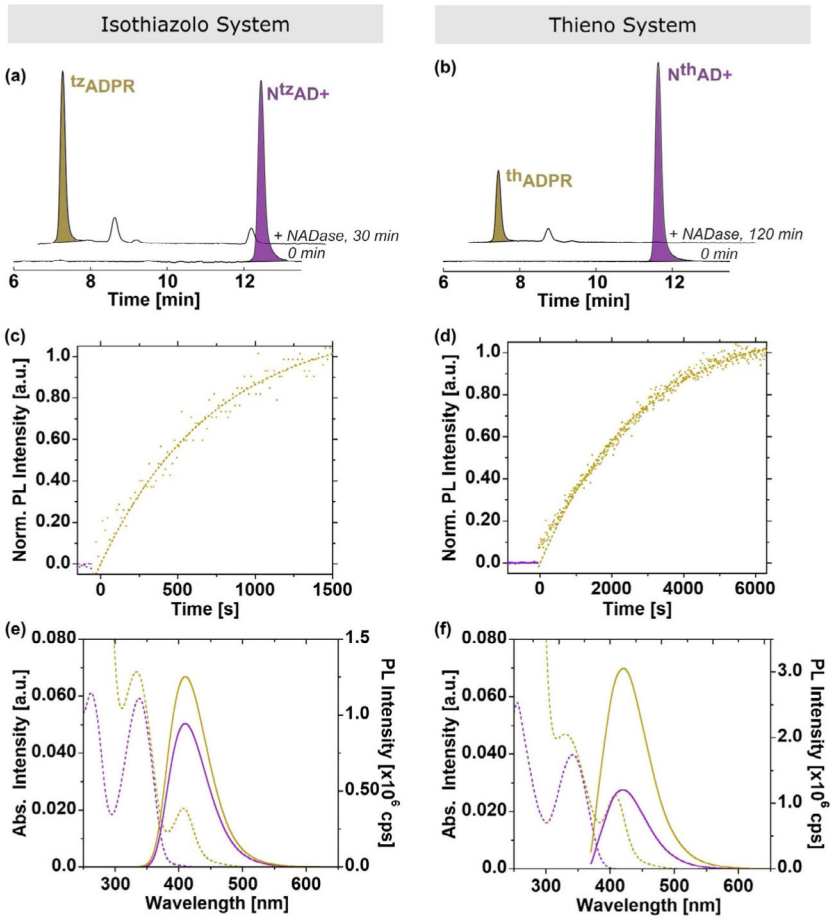

Figure 3.

Monitoring of the NADase-mediated hydrolysis of emissive NAD^+ analogues. Top: HPLC traces of (a) $\mathbf{N^{tz}AD^+}$ (purple) and $\mathbf{^{tz}ADPR}$ (yellow) monitored before and 30 min after treatment with NMNAT1 at λ_{abs} = 330 nm; (b) $\mathbf{N^{th}AD^+}$ (purple) and $\mathbf{^{th}ADPR}$ (yellow) monitored before and 120 min after treatment with NMNAT1 at λ_{abs} = 340 nm. Center: normalized emission intensity signals over time recorded for the conversion of (c) $\mathbf{N^{tz}AD^+}$ at 410 nm (λ_{ex} = 330) and (d) $\mathbf{N^{th}AD^+}$ at 410 nm (λ_{ex} = 360) before (purple) and upon (yellow) treatment with NADase. Bottom: steady-state absorption (dashed lines) and emission (solid lines) spectra for the hydrolysis of (e) $\mathbf{N^{tz}AD^+}$ (λ_{ex} = 330) and (f) $\mathbf{N^{th}AD^+}$ (λ_{ex} = 360) recorded before (purple) treatment and 25 min ($\mathbf{N^{th}AD}$: 120 min) after the addition of NADase (yellow).

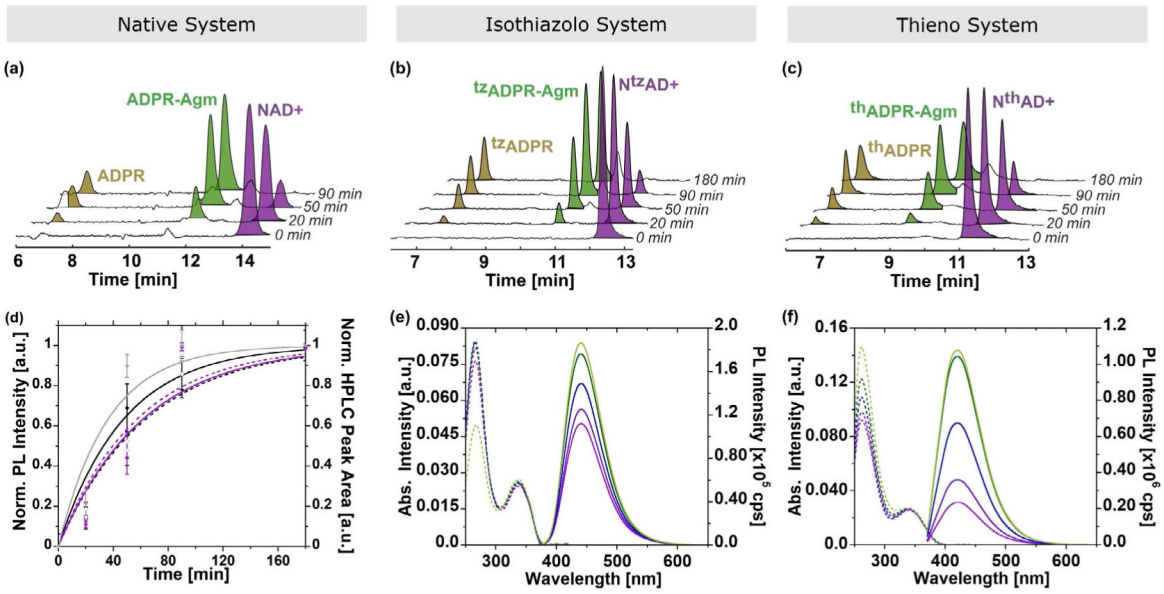

Figure 4.

Monitoring of the CTA-mediated mono(ADP-ribosyl)ation accomplished by **NAD**$^+$ and emissive analogues. Top: HPLC traces of (a) **NAD**$^+$, (b) **N^{tz}AD**$^+$ and (c) **NthAD**$^+$ (purple), agmatine adducts (green) and hydrolysis products (yellow) monitored after 0, 20, 50, 90 and 180 min at λ_{abs} = 260, 330 and 340 nm, respectively. Bottom: (d) normalized emission intensity signals (dashed lines) and HPLC peak area (solid lines) over time for the conversion of **NAD**$^+$ (grey), **N^{tz}AD**$^+$ (black) and **NthAD**$^+$ (purple); error bars refer to standard deviations of the normalized mean; steady-state absorption (dashed lines) and emission (solid lines) spectra for the conversion of (e) **N^{tz}AD**$^+$ (λ_{ex} = 330) and (f) **NthAD**$^+$ (λ_{ex} = 360) recorded after 0 min (purple), 20 min (violet), 50 min (blue), 90 min (green) and 180 min (bright green).

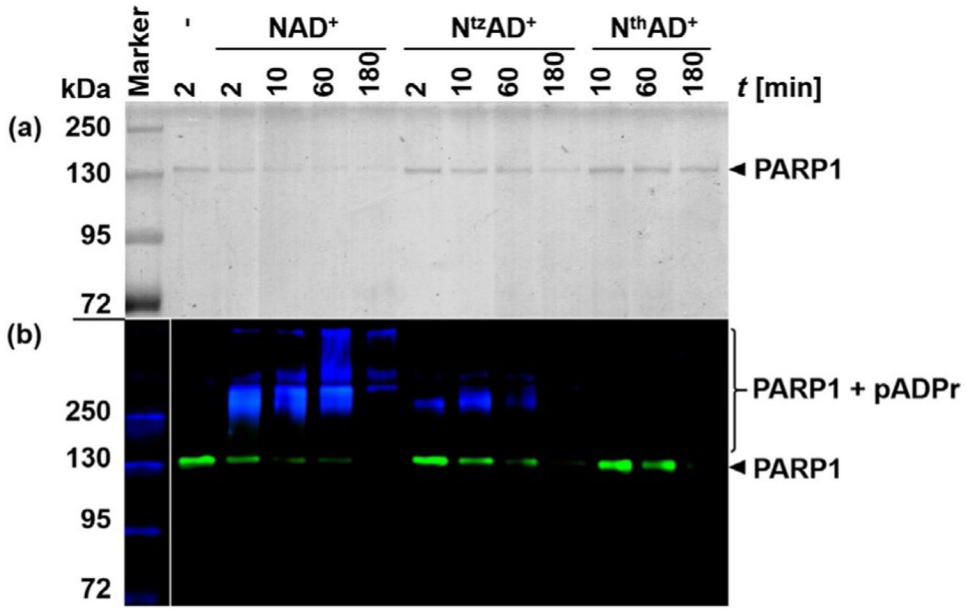

Figure 5.

(a) Coomassie stained SDS-PAGE and (b) western blot of PARP1-mediated auto-poly(ADP-ribosyl)ation reactions in presence of native **NAD**$^+$ and emissive analogues, respectively. Marker (lane 1); untreated sample (negative control, lane 2); treatment with **NAD**$^+$ (positive control, lanes 3–6), **N^{tz}AD**$^+$ (lanes 7–10) and **NthAD**$^+$ (lanes 11–13); samples were taken after 2, 10, 60 and 180 min, respectively.

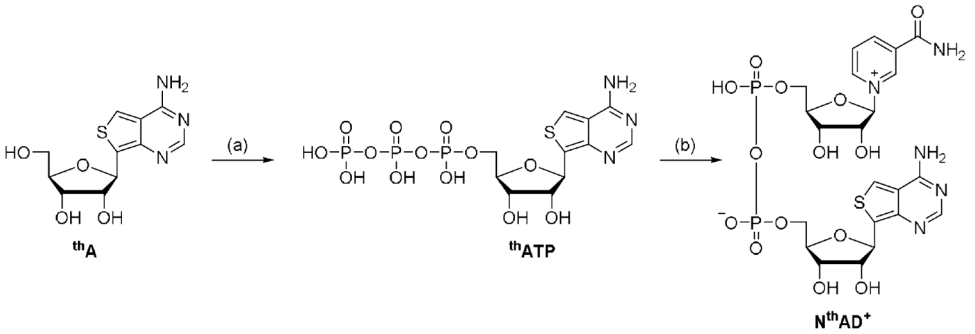

Scheme 1.

Synthesis of **NthAD^{+}**. Reagents and conditions: (a) i) TMP, $POCl_3$, 0°C; ii) tris(tetrabutylammonium) hydrogen pyrophosphate, Bu_3N, DMF, 0°C, 6.1% over two steps; (b) Tris-HCl pH 7.8, KCl, NaCl, $MgCl_2$, NMN, PPase, NMNAT1, ddH_2O, 37°C, 81%. NMN, β-nicotinamide mononucleotide; PPase, Pyrophosphatase; NMNAT1, mononucleotide adenylyltransferase 1.

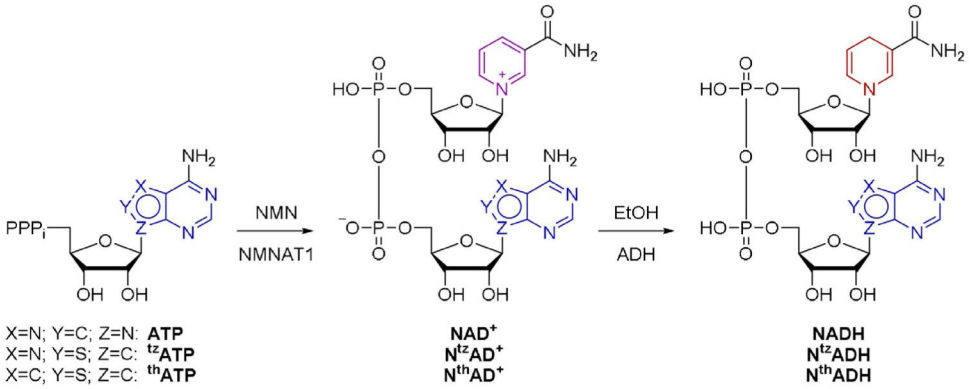

Scheme 2.

NMNAT1-mediated synthesis of native **NAD**$^+$ and emissive analogues followed by ADH-mediated reduction in the presence of EtOH. Purine and derived ring systems (blue), pyridinium (purple) and 1,4-dihydropyridine (red) moieties are highlighted. Triphosphate groups are represented by PPP_i. NMN, nicotinamide mononucleotide; NMNAT1, nicotinamide mononucleotide adenylyl-transferase 1; ADH, alcohol dehydrogenase.

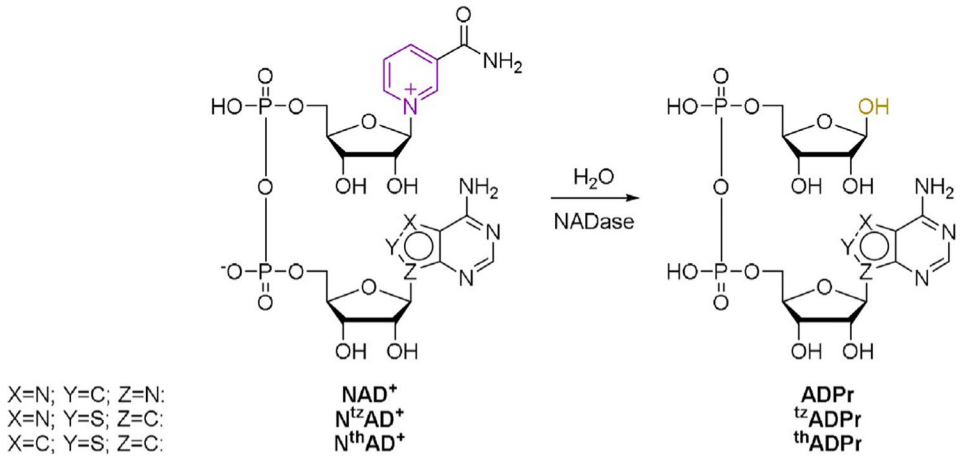

Scheme 3.

NADase-mediated hydrolysis of native **NAD**$^+$ and emissive analogues, yielding corresponding ADP-ribose (**ADPr**) species. Pyridinium moiety (purple) and anomeric hydroxy group (yellow) are highlighted. NADase, NAD$^+$ nucleosidase.

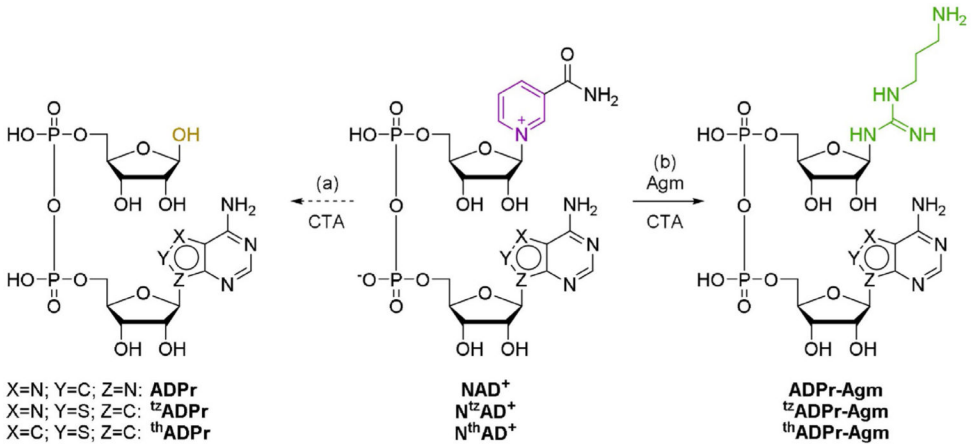

Scheme 4.

CTA-mediated conversion of native **NAD**$^+$ and emissive analogues, including (a) hydrolysis and (b) mono(ADP-ribosyl)ation of agmatine. Anomeric hydroxyl group (yellow), pyridinium (purple) and agmatine (green) moieties are highlighted. CTA, cholera toxin A; Agm, agmatine.

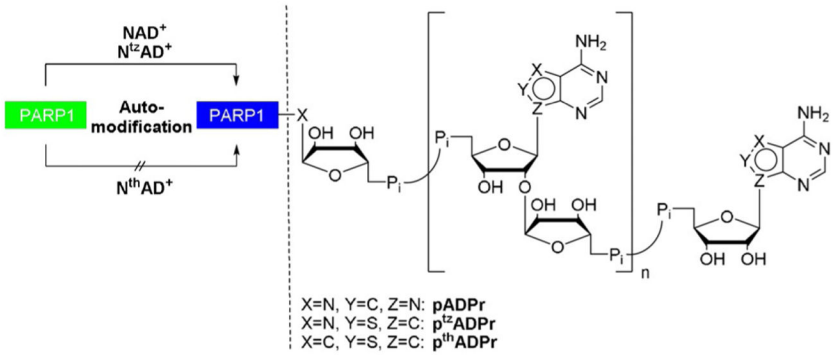

Scheme 5.

PARP1-mediated auto-poly(ADP-ribosyl)ation, facilitated by both native **NAD**$^+$ and emissive **N^{tz}AD**$^+$. Phosphate groups are represented by P_i.

Table 1.

Photophysical properties of NAD+ and its emissive analogues.

	λ_{abs} [nm]	ε [M^{-1} cm^{-1}]	λ_{em} [nm]	Φ
A[a]	260	14.9×10^3	310	5×10^{-5}
^{tz}A[a]	338	7.8×10^3	410	0.053
thA[a]	341	7.4×10^3	420	0.21
NAD$^+$[a]	259	16.9×10^3	–	–
N^{tz}AD$^+$[a]	338	7.2×10^3	411	0.044
NthAD$^+$[b]	341	7.0×10^3	431	0.071

[a]Previously reported values, see corresponding Ref. [26], [27], [29], [40], and [41].

[b]The ε value was determined at the end of NMNAT1-mediated conversion in relation to respective substrates, assuming complete consumption in 50 mM Tris-HCl buffer. All photophysical properties reflect the average of two independent measurements.